Natural Resources Canada | Ressources naturelles Canada

GEOLOGICAL SURVEY OF CANADA

OPEN FILE 7758

A 3-D compilation of data sets from the Rae craton, central Canada

D.B. Snyder, M.J. Hillier, E.A. de Kemp, J.A. Craven, and M. Pilkington

2015

Canada

GEOLOGICAL SURVEY OF CANADA

OPEN FILE 7758

A 3-D compilation of data sets from the Rae craton, central Canada

D.B. Snyder, M.J. Hillier, E.A. de Kemp, J.A. Craven, and M. Pilkington

Geological Survey of Canada, 615 Booth Street, Ottawa, Ontario

2015

doi:10.4095/295921

This publication is available for free download through GEOSCAN (http://geoscan.nrcan.gc.ca/).

Recommended citation

Snyder, D.B., Hillier, M.J., de Kemp, E.A., Craven, J.A., and Pilkington, M., 2015. A 3-D compilation of data sets from the Rae craton, central Canada; Geological Survey of Canada, Open File 7758, 1 .zip file. doi:10.4095/295921

Publications in this series have not been edited; they are released as submitted by the author.

Table of Contents

Introduction

The GEM program was designed to map Canada's North. In order to support diamond exploration, this mapping is best done at 150–300 km depths which corresponds to the so-called 'diamond window' (Griffin et al., 2004). Fully three-dimensional mapping at these depths requires geophysical methods that are calibrated by surface bedrock studies and rare mantle xenolith samples that constrain deep litho-architecture (e.g., Sanborn-Barrie et al., 2014; Petts et al., 2014). A compilation of several co-registered regional 3-D data sets now exists for the Rae craton within the Canadian Shield and can be presented in stereo using gOcad software. Ongoing diamond exploration efforts in the western Churchill region of central Canada (Hoffman, 1988) have resulted in the discovery of numerous diamondiferous kimberlite bodies that are also important xenolith host rocks. Thus, geochemistry and age of the crust can be estimated where kimberlite deposits have been discovered, crustal sample xenoliths identified and studied (Petts et al., 2014). However, mantle xenolith studies have rarely yielded pressure-temperature determinations with sufficient accuracy, or at the precision required, to unequivocally demonstrate xenolith source depth and thus evaluate diamond prospectivity or calibrate the models presented here. Our new 3-D model does provide a platform to compare 2-D geophysical information from the upper crust with sparse structural knowledge at depth, which was obtained, in part, from analysis and modelling of seismic wave observations. New insights may suggest new avenues for exploration for both diamond- and gold-rich regions.

One goal of Natural Resource Canada's GEM (Geo-mapping for Energy and Minerals) program's Diamond project was to study the deep lithosphere beneath the Slave and Churchill provinces of northern Canada. Both regions are under-going active diamond exploration, however the most prospective areas within these vast regions remains unclear. This uncertainty is a major impediment to regional target selection for follow-up diamond exploration drilling. Focusing exploration efforts on the most prospective regions reduces exploration risk and directly contributes to the competiveness of Canada's natural resource sector. From 2007 to 2012, new xenolith, seismic and magnetotelluric (MT) data were acquired and analyzed throughout the Northwest Territories and Nunavut. These data sets enhance and complement previous data of similar types as well as geologic and potential-field data sets (e.g., Hoffman, 1988; Sanborn-Barrie et al., 2014). All available data, or derived models, have been incorporated into a multi-disciplinary geoknowledge cube encompassing the central Rae craton (Figures 1 & 2).

Component data sets

Two-dimensional (near-surface maps) data

Bedrock geology

New digital geological maps of the three Canadian territories were produced within the past few years. Relevant parts were extracted and imported into the 3-D model of the Rae craton (Figure 1) (D. Paul, personal communication). Also see Berman et al. (2013) and Sanborn-Barrie et al. (2014) for further description and references on bedrock geology maps.

Gravity

Extracted from national database maintained by Canadian Geodetic Information System, Gravity & Geodetic Networks Section, Geodetic Survey Division, Geomatics Canada, Earth Sciences Sector, Natural Resources Canada.
Contact: http://gdr.agg.nrcan.gc.ca/gdrdap/dap/search-eng.php

Aeromagnetics

Extracted from national database maintained by Canadian Aeromagnetic Data Base, Airborne Geophysics Section, GSC - Central Canada Division, Geological Survey of Canada, Earth Sciences Sector, Natural Resources Canada.
Contact: http://gdr.agg.nrcan.gc.ca/gdrdap/dap/search-eng.php

Three-dimensional data

P-wave speed tomography model

Relatively short-wavelength P-waves were modeled in order to map +/- 1% variations in P-wave speed using an early, limited array of seismic stations deployed in the Rae region (Bastow et al., 2013). Such models have sufficient lateral resolution for the present applications, but very poor vertical resolution and require regularly spaced (grid) arrays to produce optimum results. A regular grid was not available for the purposes of the current study.

Surface-wave velocity tomographic models

Long-wavelength seismic waves that travel near the Earth's surface are also recorded at each station and can be used to produce alternative wave speed models of entire continents e.g., North America

(Figure 3). These updated models integrate a denser station set (Van der Lee & Frederickson, 2005; Bedle & van der Lee, 2009, Schaeffer & Lebedev, 2014). Updated models have sufficient vertical resolution for meaningful comparisons, but poor lateral resolution. Only part of the North American model within the Rae craton region was extracted and incorporated within the Rae 3-D model.

Conductivity

Earth conductivity can be estimated and modelled from magnetotelluric survey records of changes in the Earth's electric and magnetic fields over several hours to days. Recording sites in the Rae craton (Figure 2) were used to model conductivity to about 200 km depth in 2-D and 3-D (see Jones et al., 2002; Spratt et al., 2014 for description of the observations and data). The 3-D conductivity models shown here (Figure 4) were developed following methods described by Siripunvaraporn and Egbert (2009) and implemented following the approach of Roberts and Craven (2012).

Seismic discontinuities from receiver functions

Seismic discontinuities are produced by lithological changes and generally cause seismic waves to convert (P-waves to S-waves). These seismic discontinuity structures, or lithologic contacts, can be mapped in 3-D provided that stations record (in 360 compass degrees; represented here as a 3-dimensional cone) sufficient incoming earthquake waves (Figure 5) (e.g., Snyder et al., 2013). The Moho (crust-mantle boundary) is typically the strongest discontinuity within the lithosphere. Here, the estimated ray path of the seismic wave was calculated using the mean distance to earthquake sources. Seismic wave ray paths were calculated for each 5-degree azimuthal bin and only for stations that record at least 5 earthquakes. Estimated ray paths are shown as ribbons, on which bright blue or red bands mark wave conversions and potentially demarcate broad (gross?) lithologic changes. Individual seismic discontinuities were mapped by interpolating between overlapping cone coverage (Figure 5). Several distinct surfaces were mapped within the Rae craton. As expected, the Moho is clearly visible across the Rae craton (Thompson et al., 2010). In contrast, a seismic discontinuity first observed beneath the Nunuq kimberlite field, and another beneath Rankin Inlet (blue and red surfaces, respectively, in Figures 5 & 6) are shown. This second prominent discontinuity surface projects into the Central Structural Domain, which was previously identified based on gravity gradients and surface mapping of regional geological structures of (Sanborn-Barrie et al., 2014), (Figures 6 and 7).

Gravity field 'Worms'

The term ‘worming’ implies jointly plotting the maximum horizontal gradient of the gravity field continued upward to a number of elevations (altitudes) above the surface (Figure 7). For a vertical contact or lateral density contrast, the maximum gravity gradient is situated directly above the inferred contact. For more shallow-dipping contacts, the gravity maxima migrates down-dip as the assumed upward continuation elevation increases. The higher continuation elevations reflect deeper structure, but this relationship is not linear or well calibrated (Archibald et al., 1999). The color-coded depth scale in Figure 7 and the inferred surfaces based on these depth estimates are approximate.

Seismic anisotropy from SKS-splitting parameters

Seismic fabric (typically called anisotropy) can be detected where foliation, fluid-filled fractures, or dyke-like structures in rock cause much larger seismic S-waves to undergo birefringence, a phenomenon where orthogonal shear waves travel at different speeds (Silver 1996). The split or delay between arrival times provides a proxy for the degree of anisotropy, or fabric, whereas the fast polarization direction constrains the fabric plane strike. This approach can only define the geometry and characteristics of relatively simple fabrics within large volumes. Moreover, models are generally restricted to those assuming hexagonal symmetry with a horizontal axis and thus vertical fabric planes must be assumed. This type of fabric is incorporated into the 3-D models using parameters from the analysis of Snyder et al. (2013).

The Rae 3-D Compilation

The 3-D data were integrated using Paradigm gOcad version 2014.1. The integrated dataset includes the following objects: point sets (station locations, discontinuity picks, worming points), surfaces (seismic discontinuities, receiver function cones, surface geology, gravity field, aeromagnetic field) and voxets (conductivity, surface wave velocity, P-wave velocity). Some surface objects (receiver function cones, surface geology, worming points) were simply imported, whereas others (seismic discontinuities) were modeled within gOcad from point sets picked using other object features.

Users can assess the quality of the constraints on the discontinuity surfaces themselves by viewing each receiver function cone and its associated discontinuity picks before viewing the picks with the resulting surface (Figure 5). Both the accuracy and significance of a discontinuity surface can then be assessed by viewing the surface in conjunction with a voxet, such as conductivity (Figure 4), and also to

investigate possible correlations. Voxets are best viewed via three orthogonal slices: depth, north-south vertical, east-west vertical planes (Figure 4). For example, by moving these planes across the central Rae craton region, one notes that the more highly conductive areas of the mantle fall largely below the Rankin seismic discontinuity at 90–150 km depths (yellow surface on Figure 4). Here we infer that some discontinuities represent boundaries between major tectonic terranes and that enhanced conductivity, to some extent, maps the products of metasomatism. Slicing the 3-D model at major tectonic boundaries provides an opportunity to infer how the Rae craton may have been geologically assembled (Figure 8).

References

Archibald, N. J., P. Gow, and F. Boschetti, 1999. Multiscale edge analysis of potential field data. Exploration Geophysics, 30, 38–44, doi: 10.1071/EG999038.

Bastow, I.D., D.W. Eaton, J–Michael Kendall, G. Helffrich, D.B. Snyder, D.A. Thompson, J. Wookey, F.A. Darbyshire, A.E. Pawlak, 2013. Hudson Bay Lithospheric Experiment (HuBLE): Insights into Pre-cambrian Plate Tectonics and the Development of Mantle Keels. Geological Society of London, Special Publications, v. 389, first published on November 27, 2013, doi:10.1144/SP389.7.

Bedle, H., van der Lee, S., 2009. S-velocity variations beneath North America. Journal Geophysical Research 114, B07308, doi:10.1029/2008JB005949.

Berman, R. G., S. Pehrsson, W. J. Davis, J. J. Ryan, H. Qui, and K. E. Ashton, 2013. The Arrowsmith orogeny: Geochronological and thermobarometric constraints on its extent and tectonic setting in the Rae craton, with implications for pre-Nuna supercontinent reconstruction. Precamb. Res. 232, 44-69.

Griffin, W. L., S. Y. O'Reilly, B. J. Doyle, N. J. Pearson, K. Kivi, V. Malkovets, H. Coppersmith, H., and N.V. Pokhilenko, 2004, Lithospheric mapping beneath the North American plate. Lithos, 77, 873–922.

Hoffman, P.F., 1988. Subdivision of the Churchill Province and extent of the Trans-Hudson Orogen, in Lewry, J.F. And Stauffer, M.R., eds., The Early Proterozoic Trans-Hudson Orogen of North America: Geological Association of Canada, Special Paper, 37, 15 – 39.

Jones, A.G., and J.A. Craven, 2004. Area selection for diamond exploration using deep-probing electromagnetic surveying. Lithos, 77, 765 – 782.

Jones, A.G., D. Snyder, S. Hanmer, I. Asudeh, D. White, D. Eaton and G. Clarke, 2002. Magnetotelluric and teleseismic study across the Snowbird Tectonic Zone, Canadian Shield: A Neoarchean mantle suture?

Geophsyical Research Letters, 29 (17), doi: 10.1029/2002GL015359.

Petts, D.C., Davis, W.J., Moser, D.E., Longstaffe, F.J., 2014. Age and evolution of the lower crust beneath the western Churchill Province: U–Pb zircon geochronology of kimberlite-hosted granulite xenoliths, Nunavut, Canada. *Precambrian Res.*, 241, 129–145.

Roberts, B., and Craven, J. (2012). Results of a Magnetotelluric Survey in Churchill, MB: GEM Energy, Hudson Bay Geological Survey of Canada, Open File 7151, 24 pages, doi:10.4095/291442

Sanborn-Barrie, M., Davis, W.J., Berman, R.G., Rayner, N., Skulski, T., and Sandeman, H., 2014. Neoarchean continental crust formation and Paleoproterozoic deformation of the central Rae craton, Committee Bay belt, Nunavut; Canadian Journal of Earth Science, v. 51, p. 635–667.

Schaeffer, A.J., and S. Lebedev, 2014: Imaging the North American continent using waveform inversion of global and USArray data; Earth and Planetary Science Letters, v. 402, p. 26–41, doi.org/10.1016/j.epsl.2014.05.014.

Silver, P.G. 1996. Seismic anisotropy beneath the continents: Probing the depths of geology. Annual Review of Earth and Planetary Science, 24, 385–432.

Siripunvaraporn, W., Egbert, G. 2009. WSINV3DMT: Vertical magnetic field transfer function inversion and parallel implementation. Physics of the Earth and Planetary Interiors, 173, 317-329.

Snyder, D.B., R.G. Berman, J-M. Kendall, and M. Sanborn-Barrie, 2013. Seismic Anisotropy and Mantle structure of the Rae craton, central Canada, from joint interpretation of SKS splitting and receiver functions. Precambrian Res., 232, 189–208, doi: 10.1016/j.precamres.2012.03.003.

Spratt, J.E., T. Skulski, J.A. Craven, A.G. Jones, D.B. Snyder, D. Kiyan, 2014. Magnetotelluric Investigations of the Lithosphere Beneath the Central Rae craton, Mainland Nunavut, Canada. Journal of Geophysical Research, Article first published online : 19 MAR 2014, DOI: 10.1002/2013JB010221..

Thompson, D.A., Bastow, I.D., Helffrich, G., Kendall, J-M. , Wookey, J., Snyder, D.B., Eaton, D.W., 2010. Precambrian Crustal Evolution: Seismic Constraints from the Canadian Shield. Earth Planet. Sci. Lett. 297, 655-666.

Van der Lee, S., Frederickson, A., 2005. Surface wave tomography applied to the North American upper mantle. American Geophysical Union Geophysical Monograph Series 157, 67-80.

Figures

Figure 1. Location map and surface bedrock geological map of the Rae craton (GEM Tri-territorial compilation, unpublished). Elements of a new three-dimensional model of Central Rae mantle are shown here below the surface geological map. White dots are locations of teleseismic stations used in this study. CB is Committee Bay belt, CF is the Chesterfield fault, QM is the Queen Maude block, RB is Repulse Bay community; MISH is the composite lithosphere terrane called Meta-Incognito-Sugluk-Hall by Berman et al.(2013).

Figure 2. Simplified geological map of the central Rae craton (Spratt et al. 2014). Magnetotelluric (MT) and teleseismic station (with names) locations are also shown. Dashed line indicates profile of Figure 8.

Figure 3. Map of surface wave velocity model for North America (Schaeffer and Lebedev, 2014), here a depth slice at 150 km. Percentage deviations in velocity are in km/s.

Figure 4. Perspective view of 3-D conductivity model for the central Rae craton. One depth slice at about 250 km depth and two cross sections of the model are shown here. The view is from an altitude of about 50 km and from the west. Orange colors represent greater conductivities, blue greater resistivity. Two surfaces are shown for reference; CSD is the Central Structural Domain surface of Figure 6, the other is the Rankin seismic discontinuity. Green cubes and white spheres indicate magnetotelluric and teleseismic sites at the surface, respectively.

Figure 5. Illustration of Rae craton seismic discontinuities as viewed from the side (from northwest). Multi-azimuthal receiver function studies described in Snyder et al. (2013) appear here as conical sections where each ribbon represents the calculated seismic wave path within a 5º azimuthal bin for seismic waves arriving at that seismic station (here stations STLN and YBKN). Prominent, laterally consistent anomalies on each receiver function (red or blue bands) were annotated using coloured balls; all such balls were then used to fit a surface for each discontinuity. Green balls and a flat surface

represent the interpreted Moho discontinuity at 37-40 km depths, blue marks a north-dipping (‘Nunuq’) surface at 200–2500 km depths, and red marks a mid-lithosphere (‘Rankin’) discontinuity at 140–150 km depths. Note that these ‘picks’ are more widely distributed (larger diameter conical sections) with increasing depth. A few other similar surfaces (purple, green, grey, yellow) are shown beneath the Melville Peninsula (Figure 1).

Figure 6. (a) Three-dimensional model viewed from beneath Baffin Island showing a surface (yellow, 0–30 km depths) projected downward from (c) mapped regional-scale axial fold planes (Sanborn-Barrie et al., 2014) and merged into the (b) mid-lithospheric (red, 140–155 km depths) ‘Rankin’ seismic discontinuity (see Figure 5). Green cubes and white spheres indicate magnetotelluric and teleseismic sites at the surface, respectively.

Figure 7. View of the model from the west showing ‘worms’ derived from horizontal gradients in the multiply upward-continued gravity field. Gold surface was constrained by one subset of these picks and surface outcrops related to the Central Structural Domain of Sanborn-Barrie et al. (2014). More prominent ‘worms’ define the Wager Bay shear zone (WBSZ) at depths of 0-25 km. Green cubes and white spheres indicate magnetotelluric and teleseismic sites at the surface, respectively.

Figure 8. Summary interpretative cross section through the Rae region model. Section location is shown in Figure 2. Dashed and solid lines mark seismic discontinuity surfaces. Numbers are crustal ages of terranes or tectonic events (italics) in Ga (Berman et al., 2013). Metasomatism is inferred from the new 3-D conductivity model. QM is the Queen Maud block and MISH the composite Meta-Incognito-Sugluk-Hall terrane.

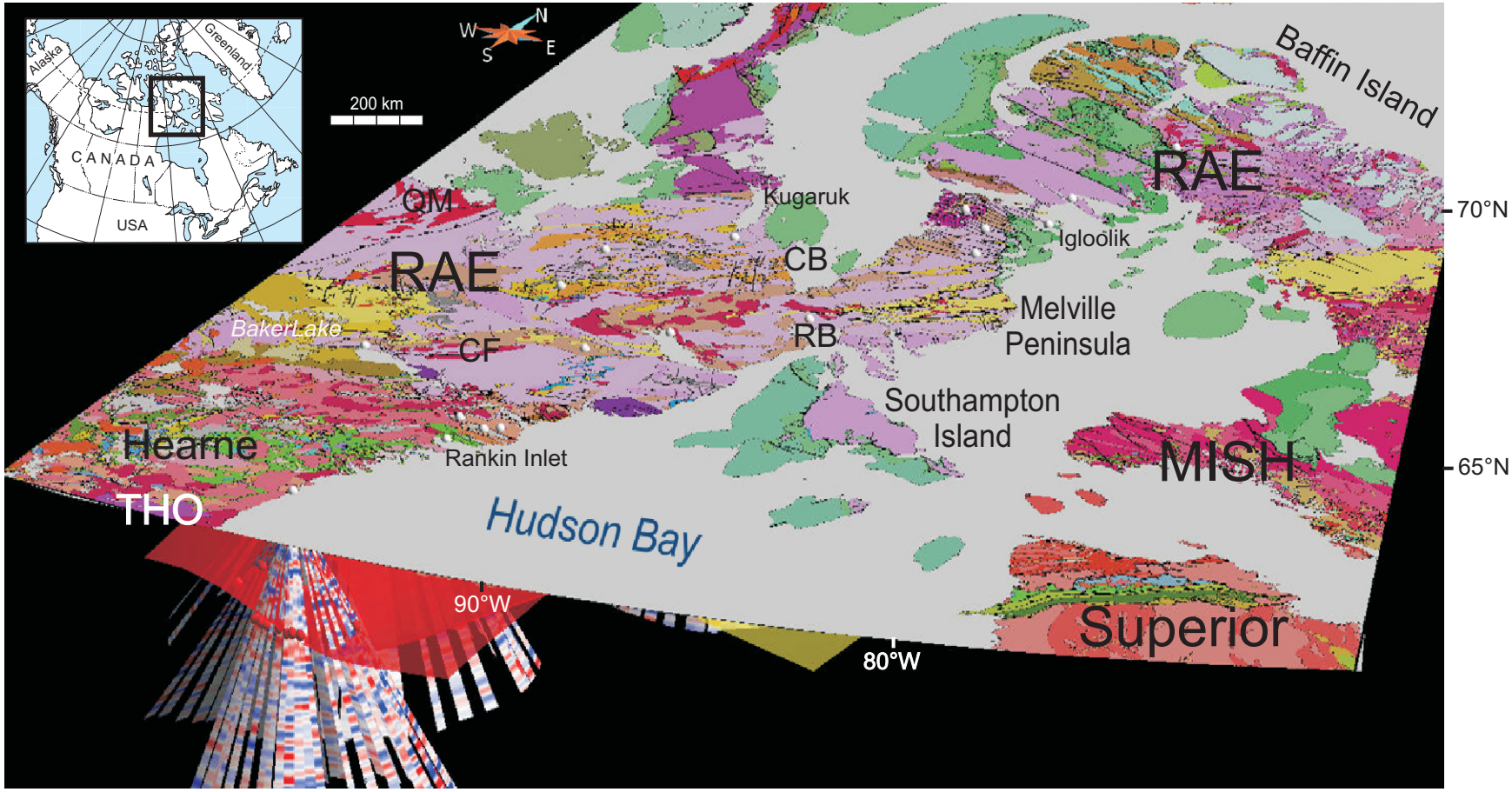
Alaska
Greenland
CANADA
USA
N
W
E
S
200 km
Baffin Island
RAE
70°N
QIM
Kugaruk
RAE
CB
Igloolik
Melville
Peninsula
RB
BakerLake
CF
Southampton
Island
Hearne
Rankin Inlet
MISH
65°N
THO
Hudson Bay
90°W
80°W
Superior

Figure 1

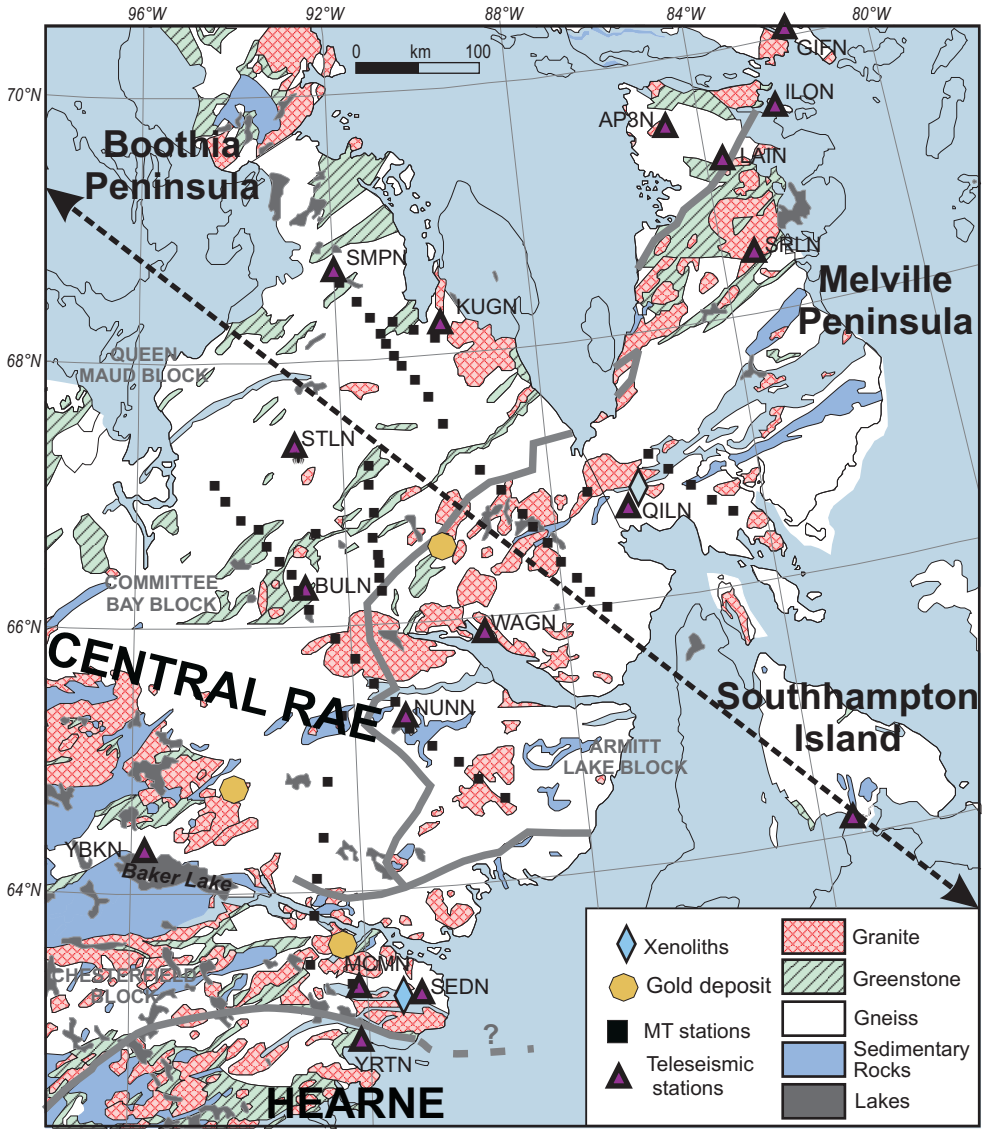
96°W
92°W
88°W
84°W
80°W
70°N
68°N
66°N
64°N
0 km 100
Boothia Peninsula
Melville Peninsula
Southhampton Island
CENTRAL RAE
HEARNE
QUEEN MAUD BLOCK
COMMITTEE BAY BLOCK
ARMITT LAKE BLOCK
CHESTERFIELD BLOCK
Baker Lake
GIFN
ILON
AP8N
LAIN
SMPN
KUGN
STLN
QILN
ABULN
WAGN
NUNN
YBKN
MCMN
SEDN
YRTN
Xenoliths
Gold deposit
MT stations
Teleseismic stations
Granite
Greenstone
Gneiss
Sedimentary Rocks
Lakes

Figure 2

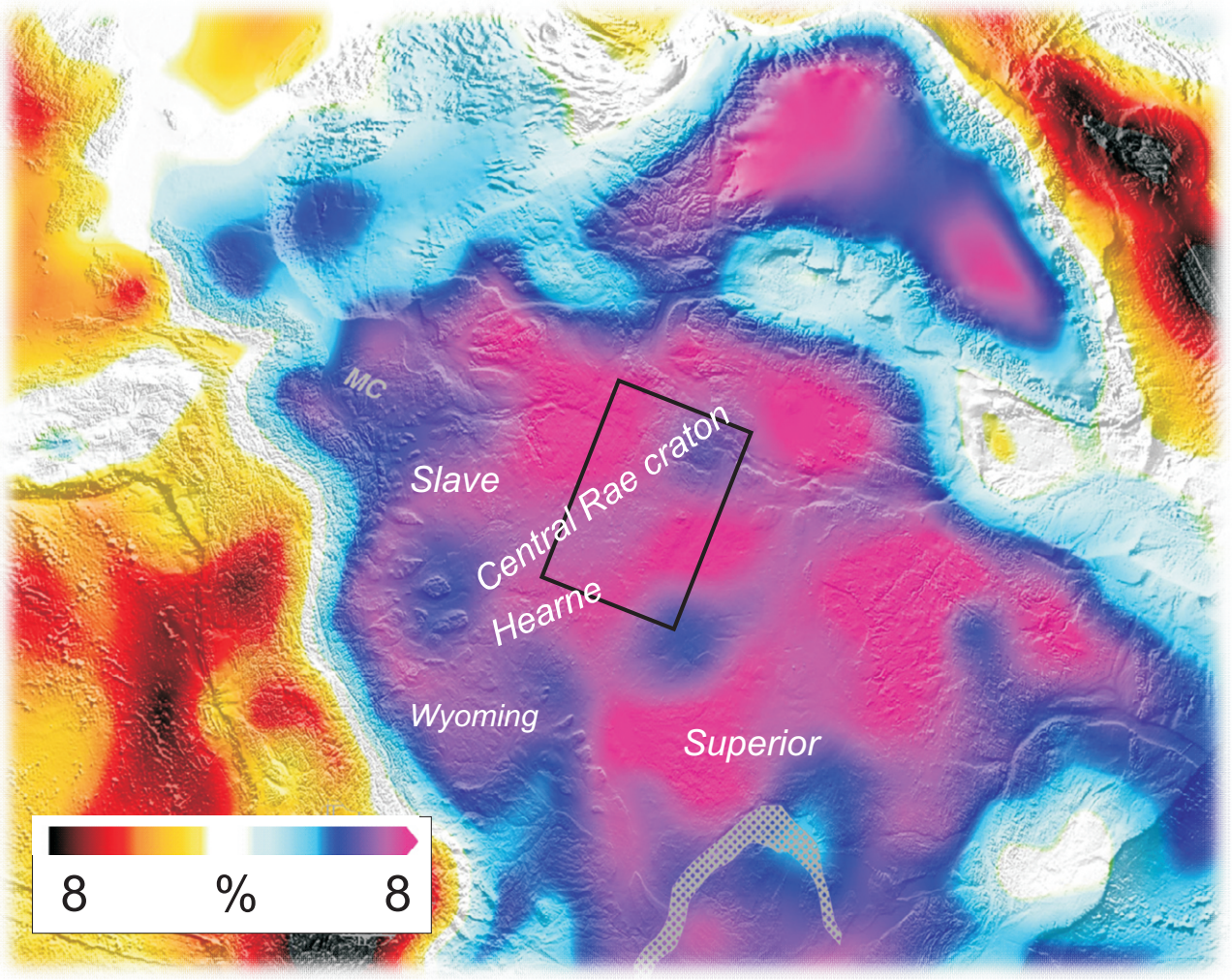

Figure 3

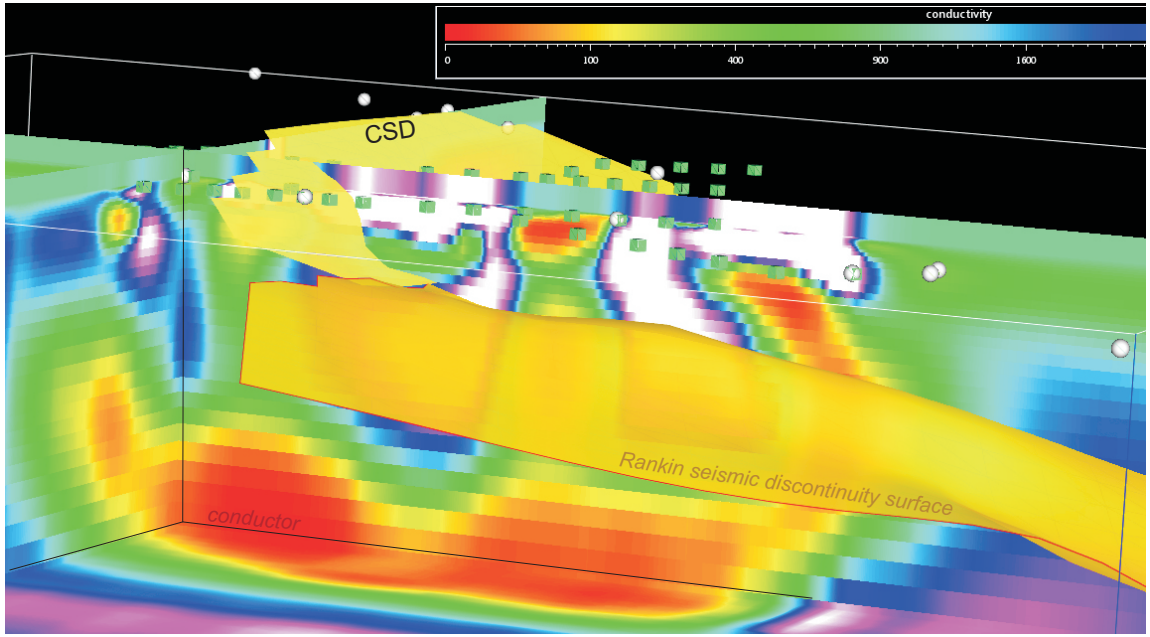
conductivity
0
100
400
900
1600
CSD
Rankin seismic discontinuity surface
conductor

Figure 4

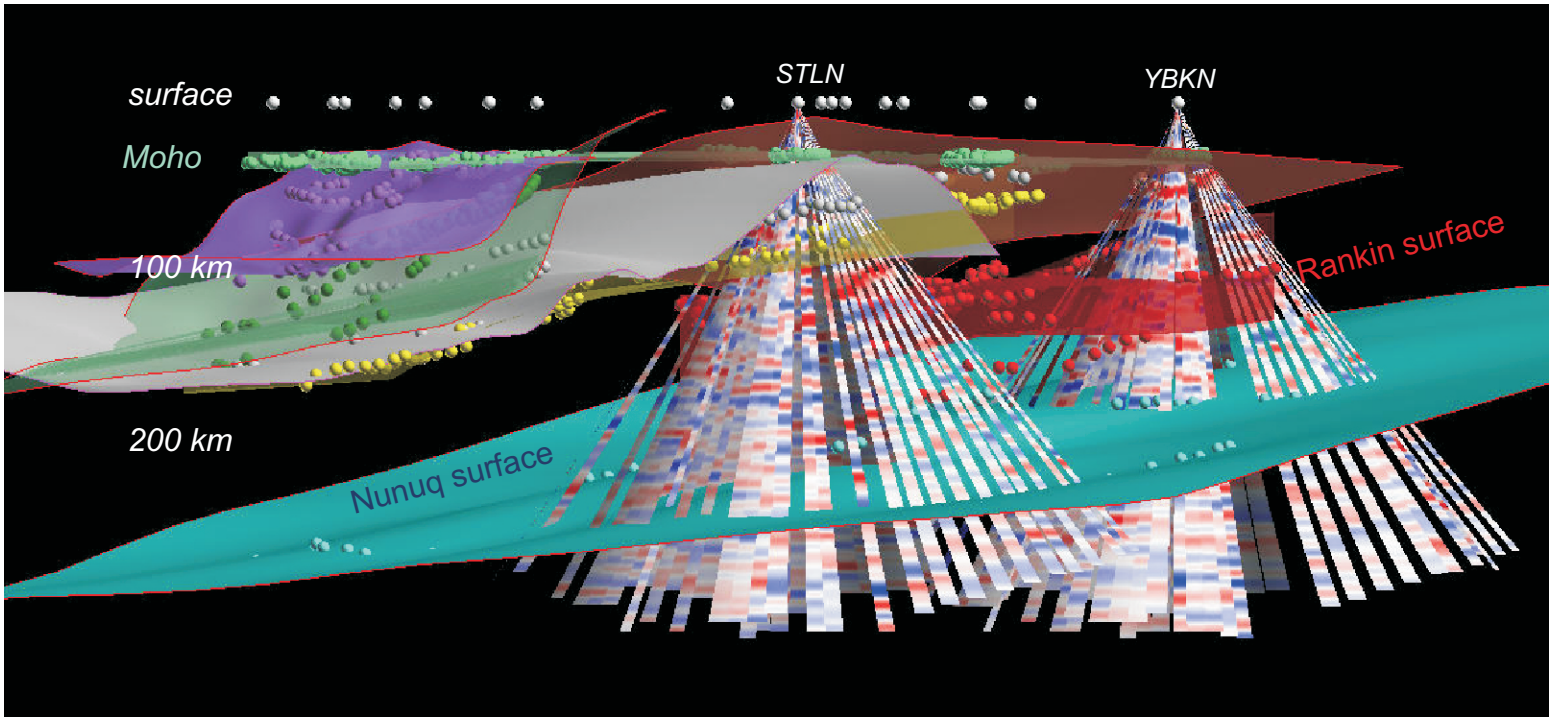
surface
Moho
100 km
200 km
STLN
YBKN
Rankin surface
Nunuq surface

Figure 5

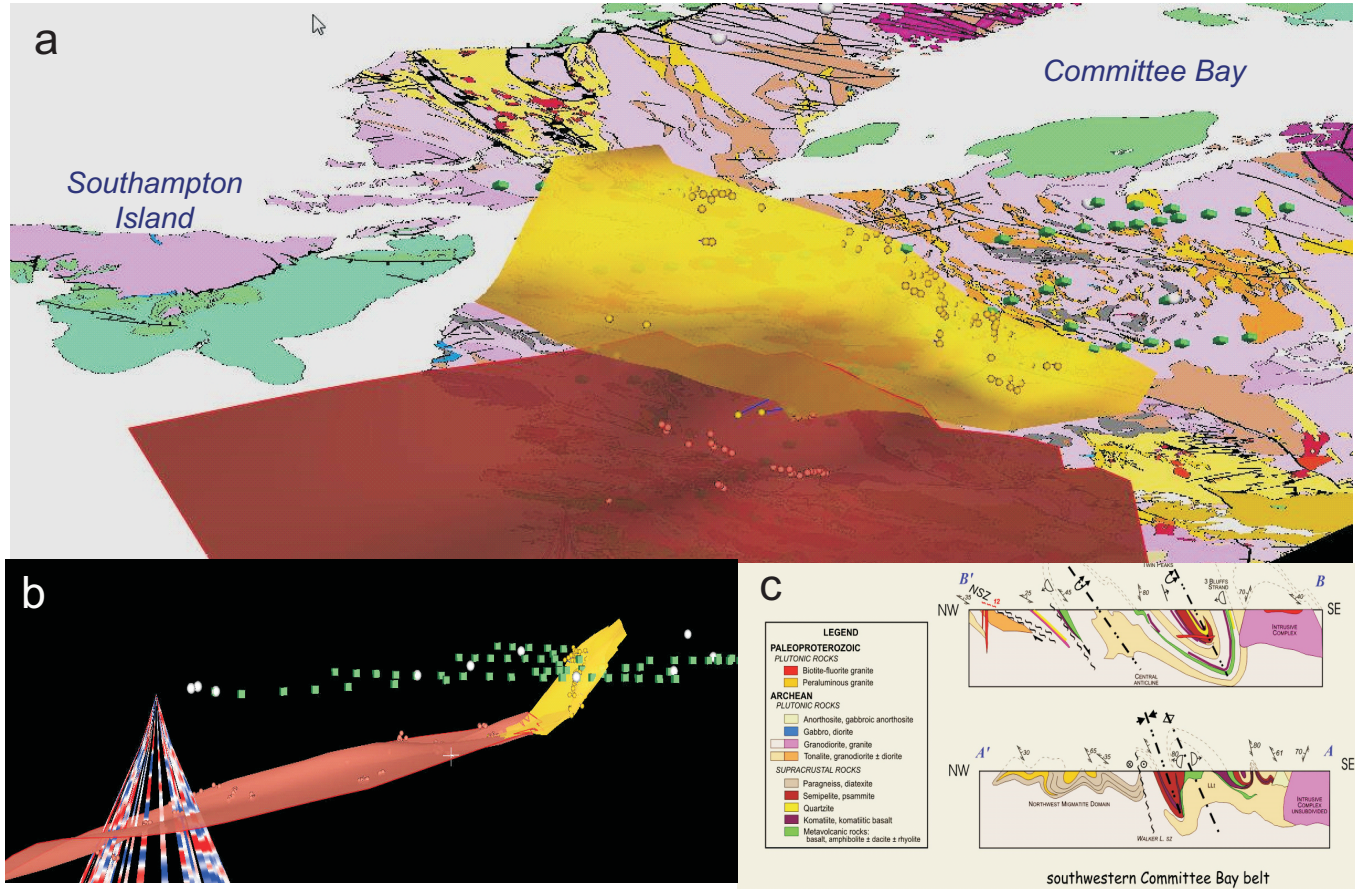
a
Committee Bay
Southampton
Island
b
c
LEGEND
PALEOPROTEROZOIC
PLUTONIC ROCKS
Biotite-fluorite granite
Peraluminous granite
ARCHEAN
PLUTONIC ROCKS
Anorthosite, gabbroic anorthosite
Gabbro, diorite
Granodiorite, granite
Tonalite, granodiorite ± diorite
SUPRACRUSTAL ROCKS
Paragneiss, diatexite
Semipelite, psammite
Quartzite
Komatiite, komatiitic basalt
Metavolcanic rocks: basalt, amphibolite ± dacite ± rhyolite
B'
NSZ
B
NW
SE
A'
A
NW
SE
southwestern Committee Bay belt

Figure 6

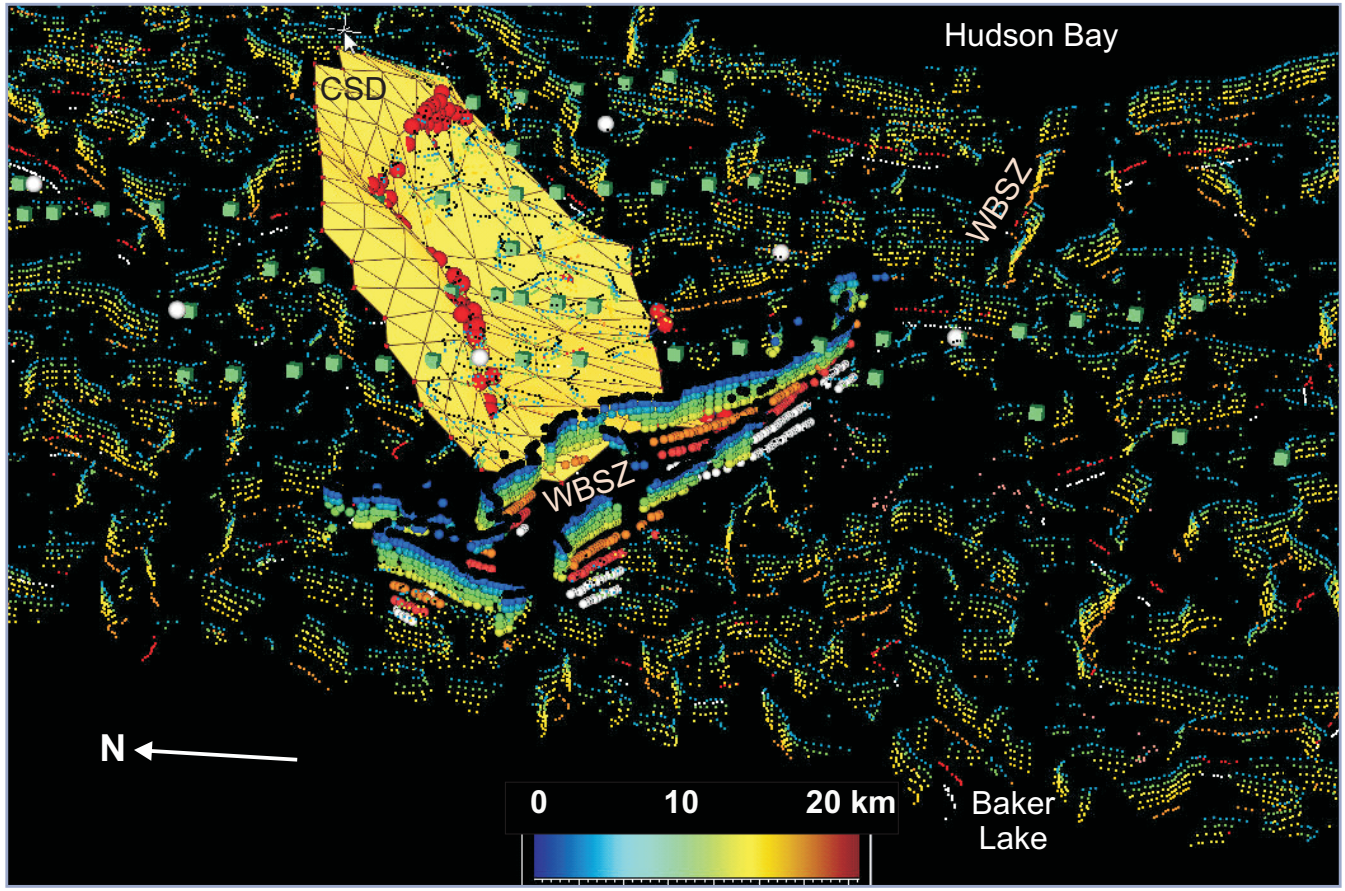

Figure 7

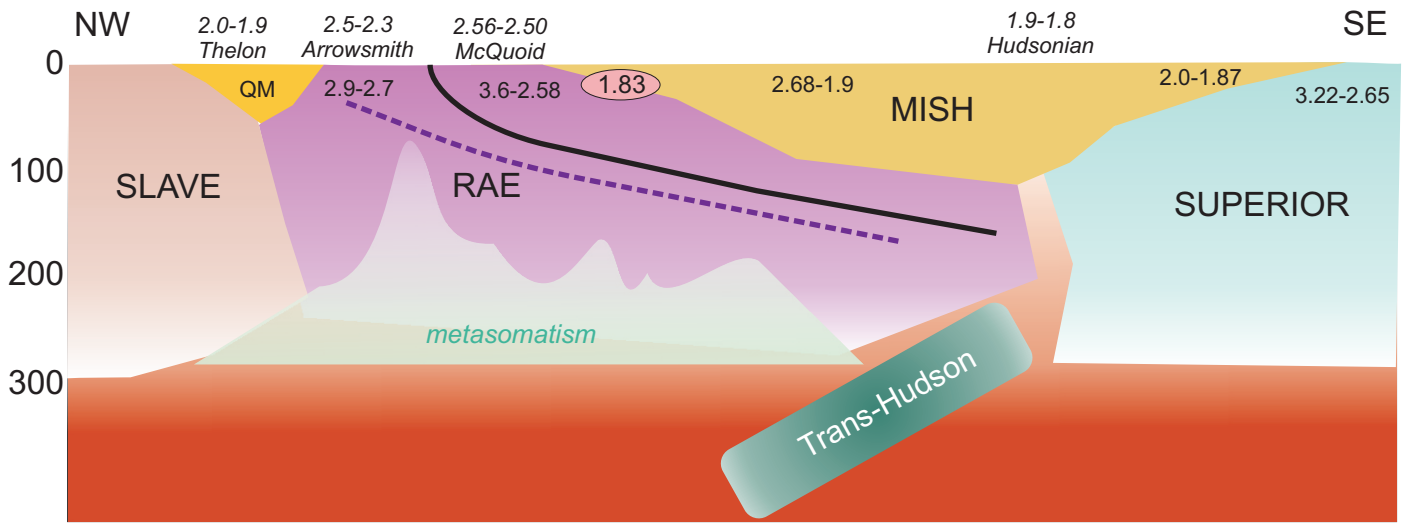
NW
SE
2.0-1.9
Thelon
2.5-2.3
Arrowsmith
2.56-2.50
McQuoid
1.9-1.8
Hudsonian
0
100
200
300
QM
2.9-2.7
3.6-2.58
1.83
2.68-1.9
MISH
2.0-1.87
3.22-2.65
SLAVE
RAE
SUPERIOR
metasomatism
Trans-Hudson

Figure 8